

Dynamics of the Reaction $O(^3P) + HBr$: Experimental Investigation and Theoretical Modeling

Kenneth G. McKendrick,[†] David J. Rakestraw, Rong Zhang, and Richard N. Zare*

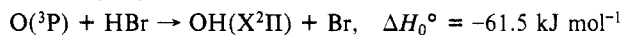
Department of Chemistry, Stanford University, Stanford, California 94305-5080
(Received: December 28, 1987; In Final Form: February 23, 1988)

The reaction $O(^3P) + HBr \rightarrow OH(X^2\Pi) + Br$ has been investigated experimentally. Two distinct approaches were pursued, differing primarily in the method of $O(^3P)$ atom production. The first involved crossing a pulsed, supersonic free jet of HBr with an effusive jet of $O(^3P)$ atoms produced by a microwave discharge in O_2 , and the second employed laser photolysis of NO_2 in a bulk mixture with HBr. The two methods gave rather similar OH product state distributions with a strong vibrational inversion ($v'' = 0, 1, 2$ in the ratio 0:9:1) and substantial rotational excitation extending to the limit of available energy. The dynamics appear consistent with expectations for the kinematically constrained reaction heavy + light-heavy \rightarrow heavy-light + heavy. Evidence was found for a contribution from reaction of $(HBr)_n$ van der Waals clusters in the crossed-beam experiments, and more authentic detailed distributions are believed to be obtained via the laser photolysis approach. Nonstatistical populations of the OH fine structure states were observed. A minor channel ($\sim 6\%$) producing spin-orbit excited $Br(^2P_{1/2})$ is proposed as an explanation for an apparent anomaly in the $OH(v''=1)$ rotational distribution. The experimental results for the $O(^3P) + HBr$ system are compared with quasi-classical trajectory calculations on a semiempirical London-Eyring-Polanyi-Sato potential energy surface, which Broida, Tamir, and Persky derived to optimize agreement between calculated and observed kinetic data. Good agreement is found between the predictions of these calculations and the experimental observations, particularly in the fractional partitioning of the energy available to the products into translation, vibration, and rotation. The $O(^3P) + HBr$ system is contrasted with previously studied reactions of $O(^3P)$ with organic molecules, in which the OH product exhibits little rotational excitation. The disparate behavior of the two systems is rationalized by consideration of the different angular dependence of model potential surfaces which satisfactorily reproduce the observed dynamics in each case.

Introduction

The reactions of electronic ground state atomic oxygen, $O(^3P)$, are of primary importance in many combustion and atmospheric processes. Consequently, a great number of studies have been reported¹⁻¹³ in which the rates of $O(^3P)$ reactions have been measured, particularly with reagents commonly encountered in combustion environments. A substantial proportion of these reactions is known to proceed by hydrogen atom abstraction, but not until relatively recently has the detailed chemical dynamics of such reactions with organic molecules been elucidated. From a series of experiments by Luntz and co-workers, a global picture was developed,¹⁴⁻¹⁷ encompassing all categories of organic molecules studied. The vibrational excitation of the OH product increases with reaction exoergicity, while in each case *very little* of the available energy appears as OH rotation.

Fairly extensive kinetic investigations of the reactions of $O(^3P)$ with *inorganic* hydrides have also been performed,³⁻⁶ and some limited information is available on the dynamics of such systems.⁷⁻¹³ However, no detailed determination of the energy partitioning in product rovibrational states has previously been reported for such a system. It is the aim of this paper to extend the dynamical understanding of hydrogen atom abstraction reactions of $O(^3P)$ to include a simple inorganic reagent, by investigating experimentally the exothermic process



This reaction is subject to an activation barrier of 14 kJ mol⁻¹, as deduced from kinetic studies,^{3,5,6} resulting in a relatively slow reaction rate at room temperature [$k(298 \text{ K}) = 3.4 \times 10^{-14} \text{ cm}^3 \text{ molecule}^{-1} \text{ s}^{-1}$]. The only previous dynamical investigation of which we are aware is the ESR flow-tube study of Spencer and Glass.¹² They concluded that a very strong vibrational inversion in the OH product occurs with over 97% formed in the first vibrationally excited level. The highly collisional conditions of such a flow-tube experiment prevented the extraction of any information on the product rotational state partitioning.

In the present study, we have employed two alternative methods for $O(^3P)$ generation. In both cases, the OH reaction product

was detected by laser-induced fluorescence (LIF). The first approach, ultimately less satisfactory with respect to the aims of this study, was conceptually similar to that employed by Luntz and co-workers in their investigations of $O(^3P) +$ organic molecule reactions.¹⁴⁻¹⁷ A pulsed, seeded supersonic free jet of the molecular reagent (in this case HBr) was crossed by an effusive jet of $O(^3P)$ produced by a microwave discharge in molecular oxygen. In addition, we have also utilized a method in which $O(^3P)$ was produced by photodissociation of NO_2 with 355-nm laser radiation. Results of this second method have been presented elsewhere¹⁸ and are therefore only summarized in this paper. The complementary information obtained in these studies will be discussed.

In a recently reported theoretical investigation, Broida, Tamir, and Persky,¹⁹ in one of a series of studies of $O(^3P)$ reactions with the hydrogen halides,²⁰⁻²³ derived a semiempirical London-Eyr-

- (1) Herron, J. T.; Huie, R. E. *J. Phys. Chem. Ref. Data* **1973**, *2*, 467.
- (2) Schofield, K. *J. Phys. Chem. Ref. Data* **1973**, *2*, 25.
- (3) Brown, R. D. H.; Smith, I. W. M. *Int. J. Chem. Kinet.* **1975**, *7*, 301.
- (4) Brown, R. D. H.; Smith, I. W. M. *Int. J. Chem. Kinet.* **1978**, *10*, 1.
- (5) Singleton, D. L.; Cvetanovic, R. J. *Can. J. Chem.* **1978**, *56*, 2934.
- (6) Nava, D. F.; Bosco, S. R.; Stief, L. J. *J. Chem. Phys.* **1983**, *78*, 2443.
- (7) Arnoldi, D.; Wolfrum, J. *Chem. Phys. Lett.* **1974**, *24*, 234.
- (8) Brown, R. D. H.; Glass, G. P.; Smith, I. W. M. *Chem. Phys. Lett.* **1975**, *32*, 517.
- (9) Karny, Z.; Katz, B.; Szöke, A. *Chem. Phys. Lett.* **1975**, *35*, 100.
- (10) Macdonald, R. G.; Moore, C. B. *J. Chem. Phys.* **1978**, *68*, 513.
- (11) Butler, J. E.; Hudgens, J. W.; Lin, M. C.; Smith, G. K. *Chem. Phys. Lett.* **1978**, *58*, 216.
- (12) Spencer, J. E.; Glass, G. P. *Int. J. Chem. Kinet.* **1977**, *11*, 97.
- (13) Agrawalla, B. S.; Manocha, A. S.; Setser, D. W. *J. Phys. Chem.* **1981**, *85*, 2873.
- (14) Andresen, P.; Luntz, A. C. *J. Chem. Phys.* **1980**, *72*, 5842.
- (15) Kleinermanns, K.; Luntz, A. C. *J. Chem. Phys.* **1982**, *77*, 3533.
- (16) Kleinermanns, K.; Luntz, A. C. *J. Chem. Phys.* **1982**, *77*, 3537.
- (17) Kleinermanns, K.; Luntz, A. C. *J. Chem. Phys.* **1982**, *77*, 3774.
- (18) McKendrick, K. G.; Rakestraw, D. J.; Zare, R. N. *Faraday Discuss. Chem. Soc.* **1987**, *84*.
- (19) Broida, M.; Tamir, M.; Persky, A. *Chem. Phys.* **1986**, *110*, 83.
- (20) Persky, A.; Broida, M. *J. Chem. Phys.* **1984**, *81*, 4352.
- (21) Persky, A.; Kornweitz, H. *Chem. Phys. Lett.* **1986**, *127*, 609.
- (22) Kornweitz, H.; Persky, A.; Levine, R. D. *Chem. Phys. Lett.* **1986**, *128*, 443.

[†] Present address: Department of Chemistry, University of Edinburgh, West Mains Road, Edinburgh EH9 3JJ, United Kingdom.

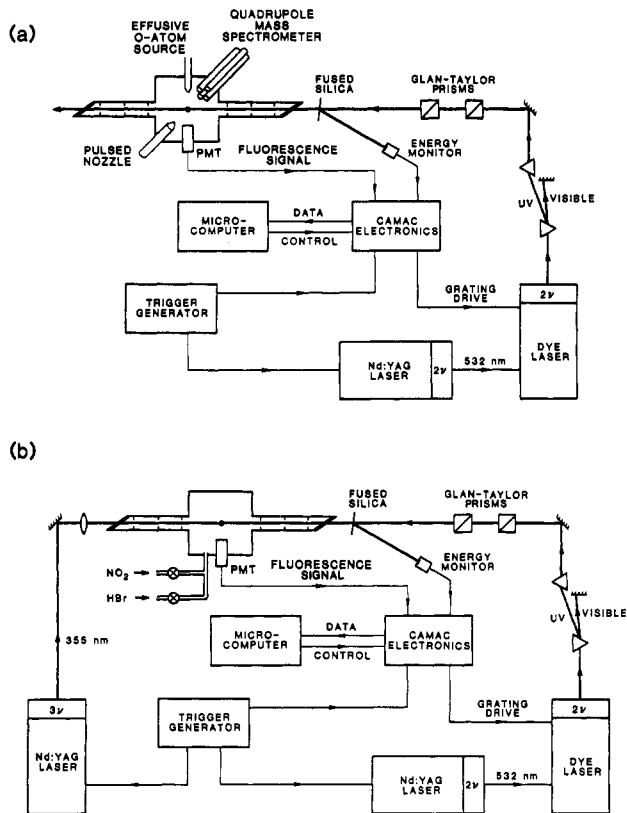


Figure 1. Schematic diagram for (a) crossed-beam and (b) laser-photolysis experimental arrangements.

ing-Polanyi-Sato (LEPS)^{24,25} potential energy surface for the O(³P) + HBr system. The Sato parameters were adjusted to optimize agreement between the results of quasi-classical trajectory (QCT) calculations and experimental kinetic data, for thermalized reagents at a range of temperatures. It should be emphasized that the dynamical information of the present study was *not* available to Broida, Tamir, and Persky at the time the surface was constructed. We present the results of extended QCT calculations, which include the computation of previously unreported rovibrational product state distributions, for initial conditions designed to match those of our experiments. Predictions of these calculations are compared to our experimental findings.

As will be made apparent below, we find very dramatic differences between the dynamics of O(³P) reactions with the previously studied organic systems, hereafter denoted as HR, and those with HBr. Both systems may be categorized generally as heavy + light-heavy → heavy-light + heavy bimolecular reactions, a kinematic combination which has received considerable experimental and theoretical attention²⁶⁻³⁴ and is the subject of substantial current interest.³⁵⁻³⁹ An explanation is offered to

account for the contrasting dynamics of the reactions O(³P) + HBr and O(³P) + HR.

Experimental Section

Two distinct experimental approaches were pursued in performing LIF measurements of OH product-state distributions, differing principally in the method of O(³P) atom production (see Figure 1). The first method (Figure 1a) will henceforth be referred to as the "crossed-beam" configuration while the second method (Figure 1b) will be designated the "laser-photolysis" configuration.

In the crossed-beam arrangement O(³P) atoms were produced by microwave discharge (OPHOS Instruments, McCarroll type cavity, 2450 MHz, 30 W), in O₂ (1–2 Torr), in a quartz glass tube external to the vacuum chamber. A trace seeding of D₂O was introduced by bubbling O₂ through liquid D₂O upstream of the discharge region, strongly enhancing the efficiency of O(³P) production. The discharge products propagated through a quartz injector tube (6-mm i.d., 25 cm long, including three 90° bends) which had been pretreated with phosphoric acid (significantly reducing heterogeneous atom recombination). The injector terminated in a 1-mm orifice through which the gases expanded to form an effusive jet in the reaction zone. The injector tip was located 8 mm below the center of the region probed by the LIF excitation beam. Evacuation through a 6-in. diffusion pump (Varian VHS6), fitted with a liquid N₂ baffle, maintained a steady-state pressure of (3–10) × 10⁻⁵ Torr in the reaction chamber, as measured by an uncalibrated ion gauge.

A pulsed, unskimmed supersonic free jet of HBr, generally seeded in He, emitted from a pulsed valve (General Valve, Series 9, 0.4-mm orifice, ~200-μs-fwhm pulse) crossed the effusive beam in the reaction region. The pulsed nozzle orifice was located 20 mm from the probed reaction region. Dilute mixtures of HBr in He were prepared in a stainless steel reservoir (500 cm³) and allowed to equilibrate for several hours prior to use.

In the laser-photolysis approach, O(³P) atoms were generated by photolysis of NO₂ in the presence of HBr (generally in a 1:1 ratio) using the third-harmonic output (355 nm) of a Nd:YAG laser (Quantel 581, 20 mJ per pulse). A pressure of 10–100 mTorr, as measured by a capacitance manometer (MKS Baratron 222BA, 0–10 Torr, absolute), resulted from the independently controlled flow of each gas and evacuation through the partially throttled diffusion pump. The photolysis beam was brought to a loose focus (spot size ~2 mm) at the center of the reaction chamber. The unfocused probe beam (spot size ~5 mm) propagated along the same axis in the opposite direction. At the short photolysis to probe pulse delay times employed in these experiments (typically 200 ns), the larger radius of the probe beam was sufficient to prevent radial loss of species produced by photolysis laser-initiated reaction.

In both experimental configurations, laser-induced fluorescence was excited by tunable ultraviolet radiation in the 280–360-nm region (bandwidth ~0.2 cm⁻¹), produced by frequency-doubling the output of a dye laser (Quantel TDL-50) pumped by a Nd:YAG laser (Quanta-Ray DCR-2A or Quantel 581). The probe laser was fired at an adjustable delay following either the opening of the pulsed HBr nozzle in the crossed-beam experiments or the firing of the photolysis laser in the laser-photolysis experiments. The crossed-beam experiments were performed at a repetition frequency of 10 Hz, and the laser photolysis experiments at 20 Hz. Probe pulse energies were varied by using a pair of Glan-Taylor prisms (allowing variable attenuation while maintaining a fixed linear polarization axis) and monitored by intercepting a partial reflection from a fused silica plate (at near normal incidence to the beam) with a joulemeter (Moletron J3-05). The

- (23) Persky, A.; Broida, M. *Chem. Phys.* **1987**, *114*, 85.
 (24) Sato, S. *J. Chem. Phys.* **1955**, *23*, 592, 2465.
 (25) Kuntz, P. J.; Nemeth, E. M.; Polanyi, J. C.; Rosner, S. D.; Young, C. E. *J. Chem. Phys.* **1966**, *44*, 1168.
 (26) Parr, C. A.; Polanyi, J. C.; Wong, W. H. *J. Chem. Phys.* **1973**, *58*, 5.
 (27) Polanyi, J. C.; Schreiber, J. L. In *Physical Chemistry, an Advanced Treatise*; Jost, W., Ed.; Academic: New York, 1974; Vol. 6A, p 383.
 (28) Baer, M. *J. Chem. Phys.* **1975**, *62*, 305.
 (29) Schulten, K.; Gordon, R. G. *J. Chem. Phys.* **1976**, *64*, 2918.
 (30) Hepburn, J. W.; Liu, K.; Macdonald, R. G.; Northrup, F. J.; Polanyi, J. C. *J. Chem. Phys.* **1981**, *75*, 3353.
 (31) Gertitschke, P. L.; Manz, J.; Römelt, J.; Schor, H. H. *J. Chem. Phys.* **1985**, *83*, 208.
 (32) Aker, P. M.; Donaldson, D. J.; Sloan, J. J. *J. Phys. Chem.* **1986**, *90*, 3110.
 (33) Schatz, G. C.; Amaee, B.; Connor, J. N. L. *Chem. Phys. Lett.* **1986**, *132*, 1.
 (34) Klippenstein, S. J.; Babamov, V. K.; Marcus, R. A. *J. Chem. Phys.* **1986**, *85*, 1924.
 (35) Firth, N. C.; Grice, R. *J. Chem. Soc., Faraday Trans. 2* **1987**, *87*, 1023.
 (36) Gertitschke, P. L.; Kiprof, P.; Manz, J. *J. Chem. Phys.* **1987**, *87*, 941.

- (37) Schechter, I.; Prisant, M. G.; Levine, R. D. *J. Phys. Chem.* **1987**, *91*, 5472.
 (38) Persky, A.; Kornweitz, H. *J. Phys. Chem.* **1987**, *91*, 5496.
 (39) Amaee, B.; Connor, J. N. L.; Whitehead, J. C.; Jakubetz, W.; Schatz, G. C. *Faraday Discuss. Chem. Soc.* **1987**, *84*.
 (40) Assignments made according to: Dieke, G. H.; Crosswhite, H. M. *J. Quant. Spectrosc. Radiat. Transfer* **1962**, *2*, 97.

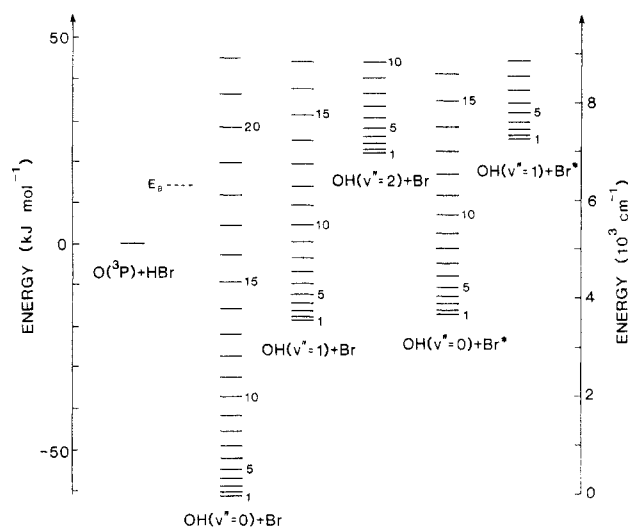


Figure 2. Energetics for the $O(^3P) + HBr \rightarrow OH(X^2\Pi) + Br$ reaction system. The $^2P_{3/2}$ and $^2P_{1/2}$ bromine atom spin-orbit states are denoted by Br and Br*, respectively. E_a is the kinetically determined activation barrier. The zero reference energy is measured in the kJ mol^{-1} scale with respect to the reagents in their lowest internal states and in the cm^{-1} scale with respect to the products in the lowest internal states.

laser axis was defined by internally baffled entrance and exit arms (1 m long) with fused silica windows set at Brewster's angle. All internal surfaces were coated with a matt black paint (Zuel Corp., St. Paul, MN). These measures were successful in greatly reducing the level of scattered laser light.

The signal collection system was also common to both sets of experiments (Figure 1). Fluorescence was detected in the vertical direction, perpendicular to the laser beam axis. A combination of fused silica lenses (effective focal length of 5 cm) imaged the reaction zone through a suitable interference filter, chosen to transmit radiation at the wavelength of the desired OH $A^2\Sigma^+ - X^2\Pi$ vibronic transition,⁴¹ onto the photocathode of a photomultiplier tube (Centronix 4283/81). Signals were captured during a 1.5- μs gate (corresponding to approximately twice the OH $A^2\Sigma^+$ fluorescence lifetime), delayed by ~ 20 ns from the probe pulse to discriminate against scattered laser light. Digitized data (LeCroy 2249SG A/D converter, CAMAC modular data bus) were transferred to a microcomputer (IBM PC-XT) for storage and analysis.

Gases used had the following stated purities: HBr (Matheson, >99.8%), NO_2 (Matheson, >99.5%), HCl (Matheson, >99.0%), O_2 (Liquid Carbonic, 99.9%), He (Liquid Carbonic, 99.9%). Liquid D_2O (Aldrich) was stated to be 99.8% isotopically pure. The NO_2 reservoir was maintained at 0 °C to ensure a stable backing pressure. HBr was freeze-pump-thaw cycled at liquid N_2 temperatures to remove dissolved H_2 .

Results

Reaction Energetics. The total energy available is the sum of the reaction exothermicity ($\Delta H_0^\circ = -61.5 \text{ kJ mol}^{-1}$) and the internal and translational energies of the reagents. Figure 2 presents a diagram showing relative energies of reagent and product states. Only the lowest $O(^3P_2)$ and $OH(X^2\Pi_{3/2})$ fine structure states are shown. Ground, $^2P_{3/2}$, and excited, $^2P_{1/2}$, spin-orbit states of the bromine atom, separated by 3685 cm^{-1} , are denoted by Br and Br*, respectively. All energies are measured relative to the lowest states of OH and Br.

In the crossed-beam experiments, the contribution to the collision energy from the HBr velocity is relatively well defined, whereas there is a broad distribution in the contribution from $O(^3P)$ atom velocities. Assuming a perfectly isentropic supersonic expansion,⁴¹ and a seeding ratio of 5% HBr in He (which is typical of these experiments), and neglecting any angular divergence of

the beam, the contribution from the (monoenergetic) HBr velocity to the center-of-mass collision energy is calculated to be 10.8 kJ mol^{-1} . In contrast, the velocity distribution of the effusive $O(^3P)$ atom beam is described by a relatively broad Maxwellian distribution. Neglecting the angular divergence, the average contribution to the collision energy is 5.0 kJ mol^{-1} , but with a substantial fraction of collisions occurring at higher energies (e.g., 1% of $O(^3P)$ atoms contribute greater than 14 kJ mol^{-1} collision energy).

Cooling in the supersonic expansion is expected to reduce substantially the rotational energy of the HBr reagent. However, as will be discussed below, trajectory calculations suggest marked promotion of reaction by HBr rotation. Despite the uncertainties in estimating the contribution from the translational and rotational energies of the reagents, an approximate value of $\sim 80 \text{ kJ mol}^{-1}$ (6700 cm^{-1}) may be estimated for the average energy available to the products for the crossed-beam configuration, with a significant fraction of available energies as much as 10 kJ mol^{-1} (840 cm^{-1}) higher than the average.

A full discussion of the reagent energies in the laser-photolysis experiments has been given elsewhere.¹⁸ From the knowledge of the O-NO bond dissociation energy⁴² and photolysis photon energy, an upper limit to the $O(^3P)$ atom velocity may be estimated. Combined with the contribution from thermal translational energy of HBr, an approximate estimate of the upper limit to the $O(^3P) + HBr$ collision energy of 25 kJ mol^{-1} (2050 cm^{-1}) is deduced. An additional 6 kJ mol^{-1} is predicted to be available from HBr rotation. The total available energy thus derived for the laser-photolysis configuration, including the reaction exothermicity, which in both experimental systems is the dominant quantity, is $\sim 92 \text{ kJ mol}^{-1}$ (7700 cm^{-1}).

On the basis of the above discussion, consideration of Figure 2 reveals that in both experimental systems a significant fraction of collisions will occur at energies above the dynamical threshold for reaction, which is estimated to be close to the kinetically determined activation energy of 14 kJ mol^{-1} .⁶

Relative Population Distributions from Intensity Measurements. OH product populations are deduced from LIF excitation spectra (fluorescence intensity as a function of probe laser wavelength). In general, an interference filter is selected to transmit only the fluorescence emitted on a specific vibronic transition: this affords the advantages of discriminating against scattered laser light and, in certain cases, of simplifying the observed spectrum. Data are generally collected on all the major branches of the A-X transition, allowing the fine structure and A-doublet substrate populations to be determined. In the reduction of observed LIF intensities to populations, account was taken of variations in the probe laser pulse energy, the wavelength dependence of the interference filter transmission, and the small polarization corrections required when exciting LIF with a linearly polarized laser.⁴³ Transition probabilities were taken from either published results^{44,45} or those kindly communicated to us in advance of publication by Copeland, Jeffries, and Crosley⁴⁶ and by Trolier and Wiesenfeld.⁴⁷

The OH A-X diagonal transitions ($\Delta v = 0$ progression) may easily be radiatively saturated with the probe pulse energies available from the dye laser system used in these experiments. A careful study of the effects of radiative saturation was performed in the laser-photolysis experimental configuration (the signal-to-noise ratio was substantially superior in this mode of operation). Measurements were made of the ratios of main branch to satellite line intensities, where the same lower state is probed with substantially different transition probabilities. Comparison with the

(42) Busch, G. E.; Wilson, K. R. *J. Chem. Phys.* **1972**, *56*, 3626.

(43) Greene, C. H.; Zare, R. N. *J. Chem. Phys.* **1983**, *78*, 6741.

(44) Chidsey, I. L.; Crosley, D. R. *J. Quant. Spectrosc. Radiat. Transfer* **1980**, *23*, 187.

(45) Dimpfl, W. L.; Kinsey, J. L. *J. Quant. Spectrosc. Radiat. Transfer* **1979**, *21*, 233.

(46) Copeland, R. A.; Jeffries, J. B.; Crosley, D. R. *Chem. Phys. Lett.* **1987**, *138*, 425.

(47) Off-diagonal band rotational line strengths used were the unpublished values of M. Trolier and J. R. Wiesenfeld.

(41) Anderson, J. B. In *Gasdynamics*; Wegener, P. P., Ed.; Marcel Dekker: New York, 1974; Vol. 4, p 1.

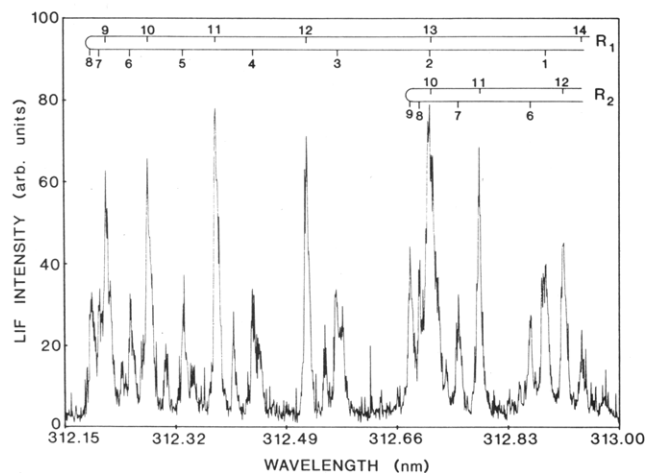


Figure 3. LIF excitation spectrum of the OH A-X (1,1) band from the reaction O(³P) + HBr in the crossed-beam arrangement. Fluorescence was selectively detected on the (1,0) band. Nozzle expansion conditions: 5% HBr in He; 2.3-atm backing pressure; 0.4-mm orifice diameter.

calculated relative transition probabilities⁴⁴⁻⁴⁷ allows the extent of saturation to be estimated.⁴⁸ It was found that, for excitation on the stronger diagonal ($\Delta v = 0$) bands, pulse energies less than 10 μ J were sufficiently low to produce an essentially linear proportionality of the observed LIF signal on the excitation pulse energy. This is in good agreement with expectations from the absolute transition probabilities and spatial characteristics of the probe pulse. For the weaker off-diagonal ($\Delta v = -1$) transitions, pulse energies less than 500 μ J were adequate for linear response.

In the crossed-beam experiments, the signal-to-noise ratio was insufficient to allow data to be collected at the limiting unsaturated pulse energy limit (although fairly reliable corrections can be applied from the empirically established extent of saturation). In any case, the principal conclusions of this study are only qualitatively dependent on the crossed-beam data: quantitative information was derived primarily from the laser-photolysis experiments.

Measured OH Product Distributions: Crossed-Beam Experiments. In a series of preliminary studies, measurements were made of the OH product-state distributions from the reactions of O(³P) with a number of organic molecules. The successful reproduction of data previously reported for these reactions, principally by Luntz and co-workers,¹⁴⁻¹⁷ provided some confirmation of the authentically nascent character of distributions measured in our crossed-beam apparatus.

Figure 3 shows a representative LIF excitation spectrum from OH($v''=1$) produced in the reaction O(³P) + HBr in the crossed-beam apparatus. R₁ and R₂ band heads of the OH A² $\Sigma^+(v'=1)$ -X² $\Pi(v''=1)$ transition [henceforth denoted (1,1)] are clearly apparent. Fluorescence was observed only on the (1,0) band, eliminating any possible congestion from lines of the (0,0) band which lie within the wavelength region containing (1,1). Rotational population distributions derived from this and similar spectra, including the other spectroscopic branches, are presented in Figure 4.

The data in Figures 3 and 4 are obtained with a seeding ratio of 5% HBr in He in the mixture expanded through the supersonic nozzle, at a backing pressure of 2.3 atm. Consideration of the data reveals substantial rotational excitation, extending to $N'' \sim 15$, with a principal maximum around $N'' \sim 11$ or 12. Considering the energy available to the products of the O(³P) + HBr reaction, it is apparent that a very substantial fraction of this energy has been channeled into internal excitation of OH.

However, there is also evidence in Figure 4 of a subsidiary population maximum in the lowest rotational states of OH($v''=1$). It was further discovered that the relative predominance of the low N'' component of the distribution was strongly dependent on

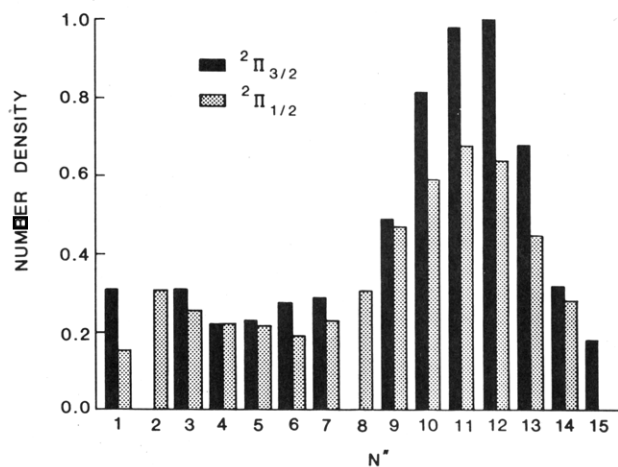


Figure 4. Relative rotational state populations of the OH($v''=1$) product in ² $\Pi_{3/2}$ (solid bars) and ² $\Pi_{1/2}$ (hatched bars) fine structure components from the reaction O(³P) + HBr in the crossed-beam arrangement. The nozzle expansion conditions are the same as in Figure 3.

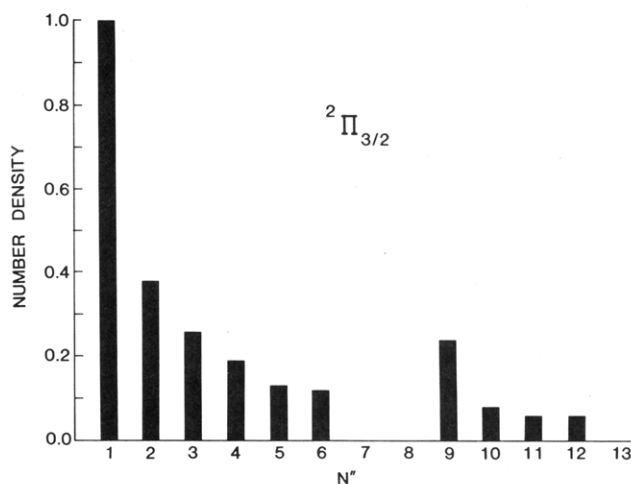


Figure 5. Relative rotational state populations of the OH($v''=1$) product in the ² $\Pi_{3/2}$ fine structure state from the reaction O(³P) + "(HBr)_n" in the crossed-beam arrangement. Rotational populations for OH($v''=1, N''=7,8$) were not measured because of spectral congestion. Nozzle expansion conditions: 100% HBr; 2.3-atm backing pressure; 0.4-mm orifice.

the dilution ratio of HBr in He in the supersonic expansion. Relative populations of the lowest N'' states were found to scale with a greater than linear proportionality to the mole fraction of HBr at a fixed total pressure. In the limit of a neat HBr expansion, with 2.3-atm backing pressure, the population distribution shown in Figure 5 was obtained. The low N'' states are seen to totally dominate this distribution.

We believe that this behavior may be explained by the formation of van der Waals clusters of HBr in the supersonic expansion, a process expected to have a higher than linear dependence on the HBr partial pressure.^{41,49-51} It has been observed for several other chemical systems that the internal excitation of a product formed in a bimolecular reaction may be significantly reduced by van der Waals clustering of one of the reagents.⁵²⁻⁵⁵ This effect is reasonably explained by partitioning of the energy available to the products of the reaction to the internal modes of the cluster.

Another interesting aspect of our observations was a strong variation of the product state distribution during the temporal

(49) Levy, D. H.; Wharton, L.; Smalley, R. E. In *Chemical and Biochemical Applications of Lasers*; Academic: New York, 1977; Vol. 2, p 1.

(50) Smalley, R. E.; Wharton, L.; Levy, D. H. *Acc. Chem. Res.* **1977**, *10*, 139.

(51) Levy, D. H. *Adv. Chem. Phys.* **1981**, *47*, 323.

(52) Nieman, J.; Naaman, R. *J. Chem. Phys.* **1986**, *84*, 3825.

(53) Naaman, R. *Laser Chem.* **1985**, *5*, 385.

(54) Nieman, J.; Naaman, R. *Chem. Phys.* **1984**, *90*, 407.

(55) Nieman, J.; Shwartz, J.; Naaman, R. *Z. Phys. D* **1986**, *1*, 231.

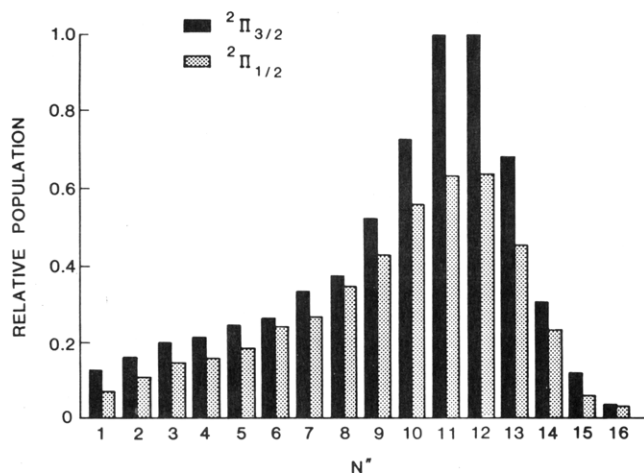


Figure 6. Relative rotational state populations of the OH($v''=1$) product in $2\Pi_{3/2}$ (solid bars) and $2\Pi_{1/2}$ (hatched bars) fine structure components from the reaction O(3P) + HBr in the laser-photolysis arrangement. Experimental conditions: 50 mTorr of HBr, 50 mTorr of NO₂; pump pulse to probe pulse delay, 200 ns.

profile of the supersonic nozzle pulse. The high N'' states (believed to be formed in the O(3P) + monomeric HBr reaction) dominated at the start and end of the pulse, with the low N'' states dominant at intermediate times. Similar, more direct measurements of time dependence of the extent of clustering in pulsed supersonic expansions have been observed previously.⁵⁶

No attempt was made to characterize quantitatively the reaction between O(3P) and (HBr)_{*n*}, primarily because there are great difficulties in attempting to determine the distribution of cluster sizes present in the expansion under a given set of conditions (or even time during the pulse). It also remained uncertain to what extent the distribution measured at the highest practicable dilution consistent with an adequate signal-to-noise ratio (5% HBr in He, Figures 3 and 4) was contaminated by the presence of HBr clusters. For this reason we consider the data obtained in the alternative laser-photolysis configuration to be fundamentally more reliable (the signal-to-noise ratio was also found to be superior). The crossed-beam data do provide, however, valuable corroborating evidence for the qualitatively accurate nature of the laser-photolysis results.

It is finally noted that no OH($v''=0$) was observable in the crossed-beam O(3P) + HBr experiments, above the residual background level. [The experimental sensitivity to OH($v''=0$) was less than that of OH($v''=1$) because OH($v''=0$) was present in the products of the microwave discharge: the magnitude of this signal was reduced but not entirely eliminated by deuteration of the seedant water essential for efficient O(3P) production.] The observation of a strong vibrational inversion in the OH product of the O(3P) + HBr reaction is consistent with the ESR measurements of Spencer and Glass¹² discussed in the Introduction.

Measured OH Product Distributions: Laser-Photolysis Experiments. The experimental results obtained by the laser-photolysis method have been described previously,¹⁸ and therefore only a summary of the salient points is presented here: Careful preliminary measurements established the regime in which the product of the pressure (P) in the reaction chamber and the time interval (Δt) between photolysis and probe laser pulses would be sufficiently low to ensure the observation of collisionally unmodified OH product-state populations. Measured distributions were essentially invariant for $P\Delta t$ less than 4×10^{-8} Torr s, and data were generally collected with $P\Delta t$ equal to 2×10^{-8} Torr s. It was also demonstrated that measured distributions were not affected by rotational-level-dependent quenching of the A $^2\Sigma^+$ state, in the range of total pressures 10–100 mTorr of a 1:1 mixture of HBr and NO₂.

Figure 6 shows rotational population distributions in the fine structure states of OH($v''=1$) derived from LIF spectra excited

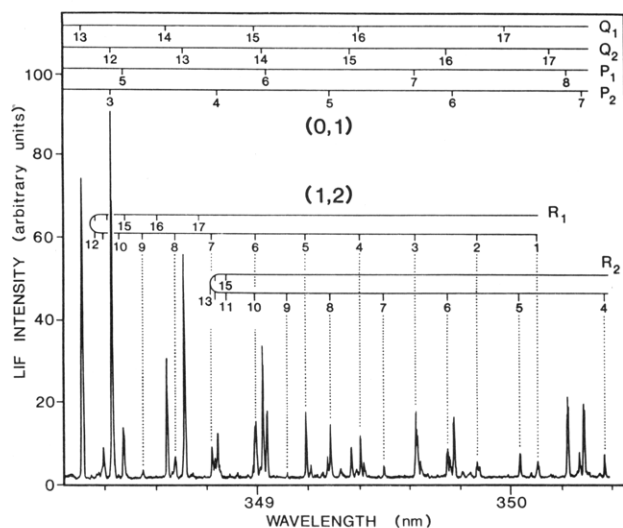


Figure 7. LIF excitation spectrum of the OH A-X (0,1) and (1,2) bands from the reaction O(3P) + HBr in the laser-photolysis arrangement. Fluorescence is observed on the (0,0) and (1,1) diagonal bands. Transitions originating from $v''=2$ are explicitly indicated by dotted lines. Experimental conditions are the same as in Figure 6.

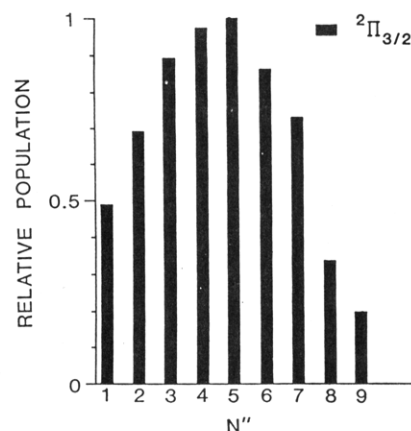


Figure 8. Relative rotational state populations of the OH($v''=2$) product in the $2\Pi_{3/2}$ fine structure component produced in the reaction O(3P) + HBr in the laser-photolysis arrangement under the conditions of Figure 6.

in the (1,1) band. As in the crossed-beam experiments, the distribution is sharply peaked with its maximum close to the highest level allowed by energy conservation (see the discussion above and Figure 2), but in contrast to Figure 4 shows only a monotonic increase in the populations of the lower N'' states.

The superior signal-to-noise ratio of the laser-photolysis experiments allowed LIF spectra to be recorded on the substantially weaker off-diagonal vibronic transitions. It is necessary to exploit an off-diagonal LIF excitation scheme to obtain information on the population of OH X $^2\Pi$ ($v''=2$), because of strong predissociation of all rotational states of A $^2\Sigma^+$ ($v''=2$).^{57–59} (The predissociation in the A state $v''=0$ and 1 levels^{57–59} occurs for rotational states above those significantly populated in the O(3P) + HBr reaction.) LIF excitation spectra of the (1,2) band were obtained while recording either the (1,0) or (1,1) fluorescence: in the latter case, lines of the (0,1) band [excited from $v''=1$] are also observed via fluorescence on the (0,0) band. Therefore, both the rotational distribution in $v''=2$ and the vibrational branching ratio ($v''=1$)/($v''=2$) may be derived.

Figure 7 shows a typical LIF excitation spectrum in the vicinity of 350 nm (in which the diagonal fluorescence was observed). Transitions originating from $v''=1$ and 2 are indicated in the

(57) Smith, W. H. *J. Chem. Phys.* **1970**, *53*, 792.

(58) Sutherland, R. A.; Anderson, R. A. *J. Chem. Phys.* **1973**, *58*, 1226.

(59) German, K. R. *J. Chem. Phys.* **1975**, *63*, 5252.

(56) Private discussions with Bruce Kay.

figure. The resultant rotational populations in OH($v''=2$), derived from this and other data, including observations of the (1,0) fluorescence, are presented in Figure 8. It is again apparent that the distribution shows a propensity for the population of levels close to the energetic limit for the O(³P) + HBr reaction.

From the data derived from spectra such as Figure 7, the vibrational branching ratio ($v''=1$)/($v''=2$) was estimated. Total populations in each state were obtained by summing over the Λ -doublet components of each fine structure state. (Those populations unavailable as a result of spectral congestion were estimated by interpolation.) The statistical accuracy of the measurements is relatively high, with $\sim 10\%$ uncertainty in the measured intensity ratios. The major uncertainty in deriving the vibrational branching ratio resulted from the accuracy of the available Einstein coefficients: the values used were those experimentally determined by Copeland, Jeffries, and Crosley.⁴⁶ The resultant branching ratio for the products of the O(³P) + HBr reaction is

$$\text{OH}(v''=1)/\text{OH}(v''=2) = 9.4 \pm 3.1 \quad (1)$$

at the 95% confidence level.

As noted previously, OH($v''=0$) is not produced at detectable levels from the O(³P) + HBr reaction in the crossed-beam experiments. In the laser-photolysis experiments, it was found that a background OH($v''=0$) concentration was generated from photolysis of HONO, formed by heterogeneously catalyzed reaction of the HBr/NO₂ mixture. Consequently, only an upper limit on the branching into OH($v''=0$) from the O(³P) + HBr reaction could be determined. A conservative estimate places this at less than 10% of the population of OH($v''=1$). This estimate is based on the assumption that the rotational states of $v''=0$ expected to be populated would be those approximately isoenergetic with the reagents (high rotational states of OH($v''=0$)), following the trend of the higher vibrational levels and the predictions of the trajectory calculations to be described below. HONO photolysis at 355 nm is known to produce OH($v''=0$) distributed predominantly in the lower rotational states.⁶⁰

Finally, the relative populations of the fine structure substates (spin-orbit and Λ -doublet components) are considered. It can clearly be seen from Figure 6 that a reproducible preference was observed in $v''=1$ for population of the lower, ² $\Pi_{3/2}$, spin-orbit state. The ratio ² $\Pi_{3/2}$:² $\Pi_{1/2}$ reaches a maximum of 1.5 at the peak of the distribution when the rotational degeneracies of the states are taken into account. A similar ratio was observed in the $v''=2$ data. The results from the crossed-beam experiments exhibit an almost identical partitioning between the higher N'' fine structure states (compare Figures 4 and 6).

No clear preference was apparent in the ratio of Λ -doublet components. Near the peak of the $v''=1$ distribution (obtained in the laser-photolysis experiments) the A' component⁶¹ was found to be favored, with a maximum ratio $\Pi(A')/\Pi(A'') = 1.2$ at $N'' = 10$. This preference rapidly declined below $N'' = 10$ and was not significant for $N'' < 7$. (The ratio is constrained to become unity in the limit of no rotation of the nuclear framework, $N'' = 1$.) We hesitate to attach too much significance to these observations, except to note that the sense of the weak preference is consistent with a dynamical constraint of the unpaired π electron in the plane of rotation of the OH molecule departing from the triatomic (O-H-Br) collision complex. Symmetry considerations obviously imply that any such Λ -doublet propensity can only result from a noncollinear O-H-Br interaction.

Discussion

Kinematic Considerations. Bimolecular reactions of the O(³P) + HBr mass combination, heavy + light-heavy (H + LH'), have been subjected to considerable experimental and theoretical sc-

rutiny.^{19-23,26-39} Certain generalizations have emerged which summarize the reactive behavior in the majority of cases. It has been found (or predicted) that a large fraction of the energy available to the products will appear predominantly as internal (rotational and vibrational) excitation. This is the result of kinematic influences rather than the topology of the potential energy surface (PES).

The excitation of product vibration can readily be understood to be the result of so-called "corner-cutting" trajectories,²⁷ in which the much more rapid motion of the light relative to the heavy atoms allows the transfer of the light atom well before the product diatomic equilibrium internuclear distance is achieved in the entrance channel. Indeed, recent collinear quantum calculations³⁶ have demonstrated that for certain H + LH' systems essentially all collinear reactive flux proceeds through corner-cutting trajectories. Gertitschke, Kiprof, and Manz³⁶ have introduced the expression "dynamical white spot" to describe the region of the potential surface which is energetically accessible but not traversed by any reactive trajectories. It is obvious from the heavily skewed character of H + LH' surfaces (when a transformation is made to mass-weighted coordinates⁶²) that a trajectory which cuts the corner will enter the exit valley with a large component of momentum perpendicular to the reaction coordinate. The products are correspondingly formed with substantial vibrational excitation.

The dynamical behavior expected for a H + LH' system may be expressed concisely in a "propensity rule"^{27,63} which predicts those product states which will be most populated

$$E_{\text{trans}}(\text{reactants}) \sim E_{\text{trans}}(\text{products}) \quad (2)$$

(where E_{trans} is the translational energy). In other words, translational energy of the reagents is expected to be converted predominantly into translational energy of the products. Orbital angular momentum will correspondingly be approximately conserved, since the reduced mass of the collision partners changes little on transfer of the light atom.

The experimentally determined OH product-state distributions for the O(³P) + HBr reaction presented above are qualitatively consistent with the propensities discussed above. The dominant product state channels are those rotational levels in OH($v''=1$) and OH($v''=2$) approximately thermonutral with respect to the reagents. On average about 75% of the available energy appears as internal excitation of the OH product. This can be compared to the analogous reaction, with a similar mass combination, F + HBr \rightarrow HF + Br,³⁰ where approximately 70% of the available energy is partitioned into vibrational and rotational excitation of HF. Rovibrational states of HF were observed up to the energetic limit for the reaction of F + HBr. This is also the case for O(³P) + HBr.

Quasi-Classical Trajectory Calculations. The extent to which the behavior of the O(³P) + HBr reaction is consistent with qualitative predictions based on kinematic constraints may be investigated quantitatively by performing QCT calculations. The assumptions inherent in this approach have been extensively discussed⁶⁴ and include the following factors: (1) the scattering system is described by a single potential energy surface; (2) quantum mechanical effects (most importantly tunneling) are unimportant, an approximation which is expected to break down near or below threshold of a H atom transfer reaction; and (3) the PES accurately describes the interaction. Assuming no attempt is to be made to describe electronic fine structure state effects, and that only energy partitioning in the nuclear degrees of freedom is to be calculated, the last of these assumptions, (3), is probably the least likely to be satisfied for the O(³P) + HBr system.

At present no ab initio calculations exist for the O(³P) + HBr potential energy surface, but a London-Eyring-Polanyi-Sato

(60) Vasudev, R.; Zare, R. N.; Dixon, R. N. *J. Chem. Phys.* **1984**, *80*, 4863.

(61) We follow the recently established notation of Alexander, M. H., et al. (*J. Chem. Phys.*, in press) in labeling the Λ -doublet components, avoiding the confusion which has arisen over the conflicting use of Π^+ and Π^- labels for these states.

(62) Kuntz, P. J. In *Dynamics of Molecular Collisions*; Miller, W. H., Ed.; Plenum: New York, 1976; Part B, p 53.

(63) Ding, A. M. G.; Kirsch, L. J.; Perry, D. S.; Polanyi, J. C.; Schreiber, J. L. *Faraday Discuss. Chem. Soc.* **1973**, *55*, 252.

(64) Truhlar, D. G.; Muckerman, J. T. In *Atom-Molecule Collision Theory: A Guide for the Experimentalist*; Bernstein, R. B., Ed.; Plenum: New York, 1979; p 505.

TABLE I: Details of LEPS Potential Energy Surfaces

	Morse parameters			Sato parameter
	$D_e/\text{kJ mol}^{-1}$	$\beta/\text{\AA}^{-1}$	$r_{eq}/\text{\AA}$	S_{ij}^c
OH ^a	446.0	2.295	0.970	0.13
HBr ^a	378.2	1.810	1.414	0.06
OBr ^a	236.0	2.462	1.717	-0.10
OH ^b	446.0	2.295	0.970	0.35
HR ^b	397.5	1.860	1.090	0.24
OR ^b	383.0	1.960	1.440	-0.15

^a From ref 19. ^b From ref 71. ^c See, for example, ref 25 for definition of LEPS surface.

(LEPS) surface, derived by Broida, Tamir, and Persky,¹⁹ is available. They adjusted the Sato parameters to optimize agreement between the results of their QCT calculations and the experimentally observed temperature dependence of the rate constant (for thermalized conditions of 200, 300, and 500 K). The values of the parameters defining the surface are reproduced for convenience in Table I. Further agreement between theory and experiment was achieved in the magnitude of the kinetic isotope effect $k_{\text{O+HBr}}/k_{\text{O+DBr}}$ and the strong vibrational inversion of OH($v''=1$) over OH($v''=0$). No detailed calculated rotational distributions were reported.

The surface of Broida, Tamir, and Persky¹⁹ has a low barrier of 13.2 kJ mol⁻¹ displaced well into the entrance channel but is predominantly repulsive; i.e., the majority of the reaction exothermicity is released in the exit channel. The surface has the minimum barrier for collinear approach of the reagents. A rectilinear potential energy contour plot for the collinear configuration is shown in Figure 9a.

The object of the present study was to extend the work of Broida, Tamir, and Persky by performing OCT calculations on their LEPS PES with specific initial conditions matching those of our experiment and, in particular, to compute detailed rovibrational product state distributions for comparison with the experimental data.

The QCT computer code used was made available to us by Professor M. D. Pattengill. Numerical integration of Hamilton's equations was achieved using a sixth-order Gear algorithm initiated by three cycles of a fourth-order Runge-Kutta-Gill algorithm. Approximately 3000 integration steps of length 0.2 fs were computed during the course of a typical trajectory, initiated at an atom-diatom separation of 7 Å. Numerical stability of the integration was verified by reduction of the constant time increment in selected batches of trajectories. Random values of the parameters required for sampling initial conditions were generated by standard Monte Carlo techniques. Calculations were performed on the San Diego Supercomputer Center Cray X-MP: the code was optimized to take full advantage of the vectorized nature of the Cray internal architecture, with parallel integration of (optimally) 64 trajectories.

As discussed, there is some uncertainty in the distribution of velocities of O(³P) atoms produced by the 355-nm photolysis of NO₂, making a rigorous simulation of the distribution of collision energies impossible. Fortunately, however, as predicted by the propensity rule (eq 2), the H + LH' mass combination results in product state distributions which are relatively insensitive to the reagent collision energy. (On increasing the collision energy from 15 to 25 kJ mol⁻¹ in our QCT calculations, the average internal energy of the products increases by only 1.3 kJ mol⁻¹.) The results reported below are derived from the unbiased averaging of the outcomes of equal numbers of trajectories at three discrete collision energies (15, 20, and 25 kJ mol⁻¹) spanning the range from slightly above the dynamical threshold for reaction to the approximate limiting collision energy in our experiment. The HBr rotational energy was specified in a quasi-classical fashion by randomly selecting a rotational quantum number from a Boltzmann distribution at 300 K.

The low reactivity of the O(³P) + HBr system in the collision energy range of interest, coupled with a relatively large limiting value of the impact parameter leading to reaction ($b_{\text{max}} = 2.5$ Å

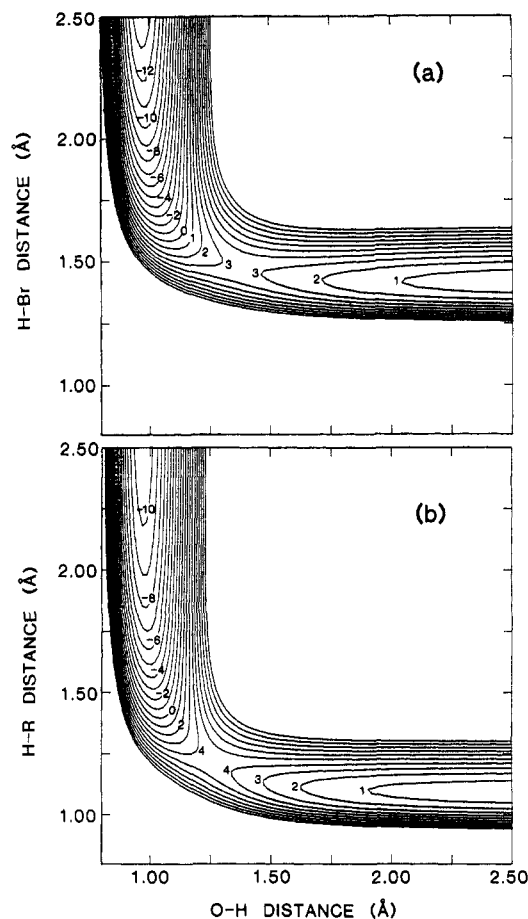


Figure 9. Contour plot of the potential energy surfaces for the collinear reactions (a) O(³P) + HBr (derived by Broida, Tamir, and Persky¹⁹) and (b) O(³P) + HR (tertiary) (derived by Luntz and Andresen⁷¹).

TABLE II: Fractional Energy Release, O(³P) + HBr

	experimental	QCT
$\langle f_{\text{vib}} \rangle^a$	0.51	0.52
$\langle f_{\text{rot}} \rangle^a$	0.24	0.22
$\langle f_{\text{trans}} \rangle^a$	(0.25) ^b	0.26

^a Fraction of available energy, excluding vibrational zero-point energy, appearing in each degree of freedom. ^b By difference.

at a collision energy of 20 kJ mol⁻¹), makes a QCT study of the product-state attributes computationally rather inefficient. The results presented below were derived from 40 000 trajectories calculated at each of the three collision energies (15, 20, and 25 kJ mol⁻¹), of which a total of approximately 1250 were reactive.

Table II contains a comparison of the fractional energy release to the vibrational, rotational, and translational degrees of freedom derived from our experimental observations and the results of the QCT calculations. It can be seen that the agreement between the calculated and observed moments of the distributions is extremely good, with, in both cases, approximately half the available energy appearing as OH vibration and the remainder equally divided between rotation and translation.

The retrospective quantization of the product-state distribution generated by quasi-classical calculation is a particularly arbitrary procedure in the present case for the vibrational degree of freedom, since the range of classical OH vibrational energies spans only about two OH vibrational quanta. Perhaps more meaningful is a consideration of the density of reactive flux into regions of classical vibrational/rotational energy space, as shown in Figure 10. It can be seen from this figure that the predominantly populated region is a sharp diagonal ridge, with a strong correlation between product vibration and rotation, and correspondingly approximately constant translational energy release. The distribution is strongly peaked in the vibrational coordinate at an energy corresponding to slightly above one OH vibrational

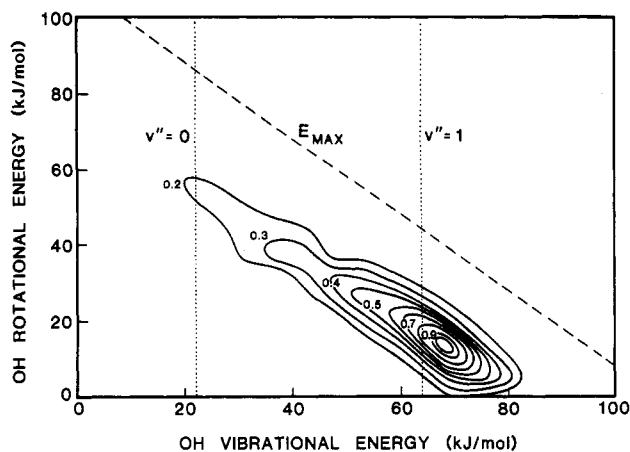


Figure 10. Contour plot of the OH reactive flux density in product vibrational/rotational energy space. The energies corresponding to OH($v''=0$) and OH($v''=1$) are indicated by dotted lines. The dashed line represents the energetic limit (E_{\max}) for the reaction. Contours represent increments of equal probability density, normalized to unity in the highest probability region.

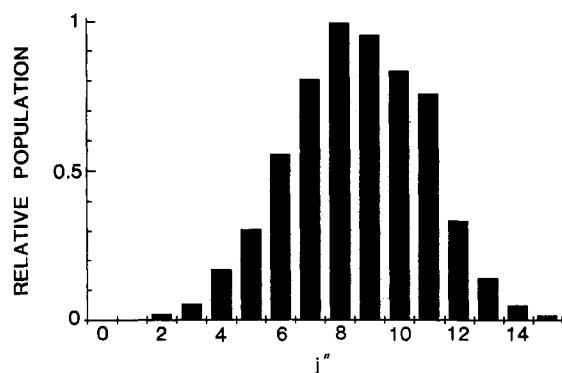


Figure 11. Calculated relative rotational state populations of OH($v''=1$) (vibrational energy corresponding to a quantum number in the range $0.5 \leq v'' < 1.5$ above the zero-point energy) derived from the results of about 1250 reactive trajectories are plotted against the pure nuclear rotation quantum number j'' . As j'' increase, j'' may be associated with N'' .

quantum (relative to the zero-point energy). Population does *not* extend to the region corresponding to OH($v''=2$), and in this respect QCT calculations run on the O(³P) + HBr surface of Broida, Tamir, and Persky fail to match the experimental observation of a branching ratio of $\sim 10\%$ into this level. The qualitative observation of a very strong vibrational inversion was reproduced, with $\sim 90\%$ of the population appearing above $v'' = 0.5$, as noted previously by Broida, Tamir, and Persky.

Quantization of the OH rotational distribution presents a less severe problem because the level spacing is relatively small compared to the range of rotational energies. The distribution for all trajectories producing OH with a vibrational energy corresponding to a quantum number in the range $0.5 \leq v'' < 1.5$ above the zero-point energy (i.e., $v'' = 1$) is presented in Figure 11. The rotational state populations are plotted as a function of the pure rotational quantum number j'' ($j'' = 0, 1, 2, \dots$), where the OH is treated as a $^1\Sigma$ molecule. The OH product molecule is actually in a $^2\Pi$ state with rotational quantum numbers $N'' = 1, 2, 3, \dots$. However, there is no direct procedure to map j'' onto N'' , although for large rotational quantum numbers $j'' = N''$. This difficulty of associating j'' to N'' has been discussed previously by Clary, Connor, and Southall.⁶⁵ Qualitative agreement with the experimentally determined OH($v''=1$) distribution is again seen to be good (cf. Figure 6), with the correct prediction of a distribution sharply peaked at a high quantum number. Quantitatively, the predicted peak of the distribution lies some one to two quanta

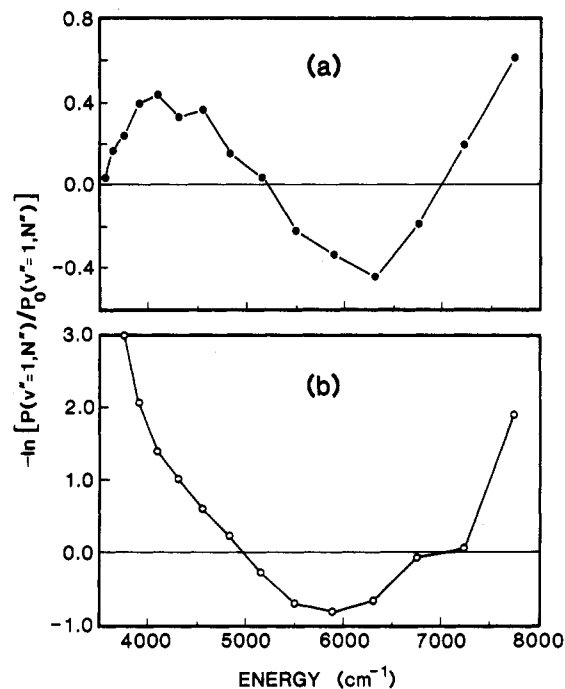


Figure 12. Surprisal plots, $-\ln [P(v''=1, N'')/P_0(v''=1, N'')]$ against total internal energy, where $P_0(v''=1, N'')$ is a prior distribution calculated purely on the basis of the density of available product states and $P(v''=1, N'')$ is the (a) experimental and (b) calculated OH($v''=1$) product rotational state distributions. The points are connected by straight lines as a guide to the eye.

below that observed experimentally. Furthermore, the population of the lower rotational states was calculated to be significantly less than was observed: the possible significance of this observation is now explored.

Evidence for Br* Production. The contrast between the experimental and calculated OH($v''=1, N''$) distribution is accentuated when the data are treated according to the "surprisal" formalism.⁶⁶ The respective distributions, $P(v''=1, N'')$, are compared with a synthetic prior distribution, $P_0(v''=1, N'')$, calculated purely on the basis of the density of available product states (neglecting angular momentum constraints). The "surprisal", $I(v''=1, N'')$, is defined by the relationship

$$I(v''=1, N'') = -\ln [P(v''=1, N'')/P_0(v''=1, N'')] \quad (3)$$

Plots of this function against total internal energy for the experimental data and the results of the QCT calculations are presented in Figure 12, a and b, respectively.⁶⁷ Both curves are markedly nonlinear (contrary to behavior found for a diverse range of other reactive systems).^{66,68} The minimum in each curve at high energy corresponds to "overpopulation", relative to statistical expectation, of the states at the peak of the distribution. This observation is essentially a restatement of the H + LH' propensity rule (2) and has been noted in surprisal plots generated in a previous theoretical study of a related system, Cl + HCl.³³

A distinct qualitative difference is apparent between the QCT results and the experimental data in the character of the low N'' regions of the surprisal plots. The subsidiary minimum at the lowest rotational state in the experimental $I(v''=1, N'')$ curve, absent from that of the QCT calculations, is equivalent to a relative

(66) Levine, R. D.; Bernstein, R. B. *Acc. Chem. Res.* **1974**, *7*, 393.

(67) The construction of a surprisal plot requires the specification of the total energy available to the products, E_{\max} . This quantity is not defined precisely for the experimental data because of the distribution over collision energies and rotational states of the reagents. In the QCT calculations, E_{\max} can be derived from an analysis of the reactive trajectories. This value, 7800 cm^{-1} , has been taken as a reasonable approximation in constructing the experimental plot, the exact form of which is only weakly dependent on E_{\max} in a reasonable range around that required for production of the highest level observed experimentally.

(68) Levine, R. D.; Bernstein, R. B. *Molecular Reaction Dynamics and Chemical Reactivity*; Oxford University Press: New York, 1987.

(65) Clary, D. C.; Connor, J. N. L.; Southall, J. E. *J. Chem. Phys.* **1986**, *84*, 2620.

excess of population in the lower rotational states in the experimental distribution. As noted in the Experimental Section, extensive measurements were performed to ensure that the observed rotational distributions were unmodified by subsequent inelastic collisions. Further corroboration for this assertion is the absence of any subsidiary maximum in the low N'' states of OH($v''=2$), shown in Figure 8. We propose that the apparent anomaly may be indicative of a subsidiary reactive channel producing these states in conjunction with spin-orbit excited Br($^2P_{1/2}$). An examination of the energy diagram (Figure 2) reveals that if an equivalent effective energetic limit to that of the ground-state Br channel is assumed, then rovibrational states OH($v''=1, N''\leq 7$) would be expected to be accessible in conjunction with Br($^2P_{1/2}$). The inflection in the $I(v''=1, N'')$ plot for the experimental data (Figure 12a) is quite consistent with this proposition.

If the $I(v''=1, N'')$ experimental curve is extrapolated to low N'' in a monotonic fashion, as suggested by the behavior of the surprisal of the QCT results, then a branching ratio of ~ 0.06 for the "extra" low N'' population may be deduced from the resultant difference between the actual and the extrapolated curves. In other words, if the above argument about the origin of this population is valid, the data indirectly indicate a branching of approximately 6% into the spin-orbit excited state Br($^2P_{1/2}$).

In principle, an attempt could be made to measure directly this branching ratio by one of several spectroscopic techniques, as has been done, for example, for the closely related reaction $F + HBr \rightarrow FH + Br^*/Br$, where the Br^*/Br ratio was found to be 0.056 ± 0.004 at room temperature.³⁰ We have not attempted such a measurement.

Influence of $O(^3P)$ Atom Fine Structure on Reactivity. The electronically adiabatic correlations in the $O(^3P) + HBr$ system are relatively complex: three spin-orbit states of the reagent $O(^3P_J)$ are coupled to two 2P_J states of the Br atom and two $^2\Pi_O$ states of OH. An argument of partial electronic adiabaticity was previously presented by Andresen and Luntz¹⁴ as an explanation for the nonstatistical fine structure state partitioning in the $^2\Pi$ states of OH produced in the reactions of $O(^3P)$ with organic molecules. However, in contrast, Polanyi and co-workers³⁰ were able to demonstrate that the Br^*/Br ratio was *not* determined by the reagent F^*/F ratio in the $F + HBr$ reaction. They argued that the product state partitioning must therefore be controlled by nonadiabatic couplings in the exit channel region of the surface.

As noted in the Results section, we observed nonstatistical and essentially identical ratios of the OH spin-orbit states in both the laser photolysis and crossed-beam experiments. The $O(^3P_J)$ distribution in the crossed-beam experiments will be that of a thermalized sample, as a result of many gas-phase and wall collisions downstream of the discharge. Unfortunately, the $O(^3P_J)$ distribution from 355-nm photolysis of NO_2 is unknown, but it would be highly coincidental if it were to be identical with the 300 K thermal distribution. It seems, therefore, more probable that the OH fine structure partitioning is *not* controlled by the reagent fine structure populations in the $O(^3P) + HBr$ system.

Similarly, it would be interesting to assess any dependence of the Br^*/Br ratio on the method of $O(^3P)$ atom production. However, as has been discussed extensively above, the low N'' OH population distribution, from the analysis of which we are indirectly deducing possible Br^* production in the laser photolysis experiments, is strongly perturbed in the crossed-beam experiments by a contribution presumed to be the result of $O(^3P)$ atom reaction with HBr van der Waals clusters. We are therefore prevented experimentally from making such a determination. An interesting extension to this work would clearly be to examine in more detail the dependence of the product fine structure state partitioning on controlled reagent fine structure populations.

Comparison of $O(^3P) + HBr$ and $O(^3P) + HR$. As noted in the Introduction, a comprehensive series of dynamical investigations of the reactions of $O(^3P)$ atoms with organic molecules has been carried out.^{14-17,69-71} It is found that these reactions

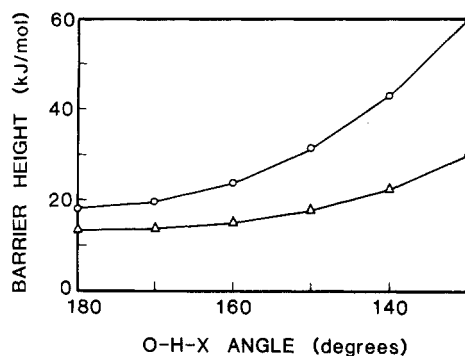


Figure 13. Variation of the saddle-point energy (barrier height) as a function of the O-H-X angle, where Δ denotes X = Br and O denotes X = R (tertiary).

exhibit the following dynamical behavior:

(i) As the reaction exothermicity increases, the energy available to the products is increasingly channeled into OH product vibration, consistent with the decline in the height of the barrier and a shift of its position into the entrance channel. For example, reaction with primary, secondary, and tertiary C-H bonds clearly exhibits this trend.

(ii) For all organic reagents studied, and essentially independent of product-state vibrational level, the OH produced is extremely "cold" rotationally. As little as 2% of the available energy typically appears as OH rotational excitation.

The second of these observations is somewhat surprising, being contrary to the general propensities for the H + LH' kinematic category discussed above. In particular, it is markedly different from the behavior reported in this paper for the reaction $O(^3P) + HBr$. We attempt to rationalize this contrast.

Luntz and Andresen⁷² were able to reproduce quite satisfactorily the qualitative and quantitative trends in their experimental dynamical data using QCT calculations on a series of related model LEPS potential energy surfaces. The reactions of $O(^3P)$ with saturated hydrocarbons were treated as pseudotriatomic O + HR systems, with R considered to be a structureless particle. The LEPS parameters were adjusted such that QCT calculations would reproduce limited aspects of the experimental results. Subject to these limited constraints, the model was capable of relatively good global prediction of the dynamics of all classes of saturated hydrocarbons (primary, secondary, and tertiary).

A potential energy contour plot, for collinear O atom approach, of the Luntz and Andresen LEPS surface for $O(^3P) +$ a tertiary hydrocarbon⁷³ is shown in Figure 9b: the parameters required to specify the surface are reproduced in Table I, facilitating comparison with the O + HBr LEPS surface. There is a distinct qualitative similarity between the two surfaces as plotted in the conventional collinear O-H-X (X = Br, R) configuration (the minimum-energy pathway in both cases). Both have barriers displaced into the entrance channel (slightly more so for O + HBr than O + HR), and the majority of the chemical energy is released (repulsively) in the exit channel. Collinear plots such as those of Figure 9a,b provide no insight, however, into the probability of rotational excitation of the products of the respective reactions. Much more enlightening is a consideration of the *angular dependence* of the surfaces, since O-H-X bending motions correlate asymptotically with OH product rotation.

The variation of the saddle point energy (with respect to the reagents) on each of the surfaces as a function of the O-H-X angle is shown in Figure 13.⁷⁴ It can be seen that the barrier height

(70) Dutton, N. J.; Fletcher, I. W.; Whitehead, J. C. *J. Phys. Chem.* **1985**, *89*, 569.

(71) Barry, N. J.; Fletcher, I. W.; Whitehead, J. C. *J. Phys. Chem.* **1986**, *90*, 4911.

(72) Luntz, A. C.; Andresen, P. *J. Chem. Phys.* **1980**, *72*, 5851.

(73) The extensions to Luntz and Andresen's work which we describe in this section are based (loosely) on a tertiary hydrocarbon with the mass of 2,2,4-trimethylpentane. This choice was motivated by the fact that we had obtained experimental results for reaction with this molecule during early experiments to verify the correct operation of our apparatus.

(69) Dutton, N. J.; Fletcher, I. W.; Whitehead, J. C. *Mol. Phys.* **1984**, *52*, 475.

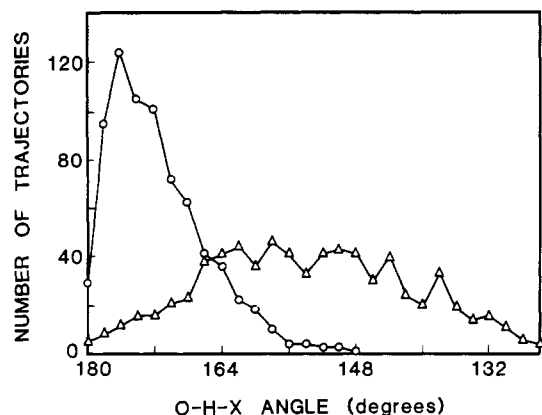


Figure 14. Calculated distributions of O-H-X angles at the "transition state", defined here as $(r_{XH} - r_{XH}^{eq}) - (r_{OH} - r_{OH}^{eq}) = 0$, where Δ denotes X = Br and O denotes X = R (tertiary).

increases *significantly more rapidly* with bending angle for the O + HR surface than for O + HBr. This observation is critical for the rationalization of the contrasting dynamical behavior of the two systems within this triatomic model treatment. As discussed above, the H + LH' mass combination results in inefficient conversion of reagent orbital angular momentum into product diatomic rotational angular momentum. Rotation of the HL product derives chiefly from the repulsive interaction in the breaking L-H' bond. Because the center-of-mass of the HL product lies very close to the heavy particle, forces acting on the light end of the molecule, through *bent* geometries, impart a large torque and efficiently convert the repulsive energy into product rotation.³³ The more rapid increase of the barrier height for O + HR restricts more severely the range of energetically accessible transition-state geometries. Consequently, the reactive flux is channeled through configurations with a narrower distribution about the collinear minimum-energy path.

Confirmation of this qualitative argument is provided by an analysis of the reactive trajectories for each system. Following Luntz and Andresen⁷² we define (loosely) the reaction coordinate, Q , according to the expression

$$Q = (r_{XH} - r_{XH}^{eq}) - (r_{OH} - r_{OH}^{eq}) \quad (4)$$

The point at which the reaction occurs is taken to be the first change in sign (from negative to positive) of the value of Q . Figure 14 shows the distribution of O-H-X angles at the point $Q = 0$ for ensembles of representative reactive trajectories in the O + HR and O + HBr systems. The narrow distribution for O + HR has been noted previously:⁷² virtually all trajectories proceed through a geometry within 20° of collinearity. In contrast, the distribution for O + HBr is much broader, extending to configurations bent by as much as 50°!

In a slightly more conventional representation,⁶² the contrasting angular dependence of these potentials is illustrated in Figure 15a,b, in which the X-H distance is fixed at the value of the saddle-point geometry. The contours represent the energy for location of the O atom at the corresponding position in the plane. The locus of the saddle-point O-H distance is also indicated. It can be seen that the O + HBr surface demonstrates a relatively shallow gradient in the potential for small excursions from a collinear geometry in the vicinity of the saddle point. However, for O + HR the gradient is significantly steeper (as is shown explicitly in Figure 13) and, furthermore, at longer range contains a large component orthogonal to the collinear axis. Therefore, it is expected that there will be a significant orientational effect for the O + HR reaction directing trajectories toward a collinear geometry, which will be absent in the O + HBr system. Analysis of the courses of representative batches of individual trajectories

(74) The slightly higher absolute value at the collinear configuration for the O + HR surface is not relevant to the present argument. We note that there is a discrepancy between Figure 13 and the original Figure 2 of ref 71, which results from incorrect construction of the original figure. The variation with angle for the O + HBr surface was given in Table 5 of ref 19.

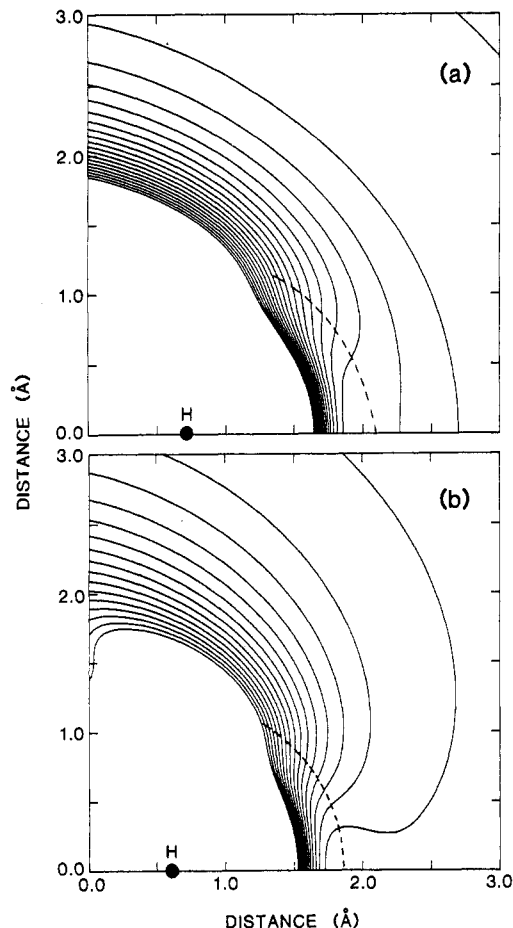


Figure 15. Contour plots showing the angular dependence of the O(³P) + HX potential energy surfaces, where (a) X = Br and (b) X = R (tertiary). The HX distance is fixed at the value of the collinear saddle point, r_{HX} . The H atom is located at the point $[(1/2)r_{HX}, 0]$, as indicated, and the X atom (not shown) is correspondingly located at $[-(1/2)r_{HX}, 0]$. Contours represent the energy for location of the O(³P) atom at the corresponding points in the plane. The loci of the O(³P) atom saddle-point distances are indicated by dotted lines.

confirmed this indeed to be the case. Active orientation by the potential therefore contributes significantly to the exceptionally narrow distribution of O-H-R angles for reactive trajectories in Figure 14. Thus, we believe the "cold" OH product rotational distribution for O(³P) + HR arises from nearly collinear H atom transfer, tightly restricted by the angular dependence of its potential energy surface. In contrast, the "hot" OH product rotational distribution for O(³P) + HBr arises from a large contribution from H atom transfer through bent geometries, facilitated by the relatively shallow gradient of the potential with respect to the O-H-Br angle. Similar contrasting angular dependencies have been observed by Persky and Kornweitz³⁸ for several different surfaces describing the hydrogen transfer reaction $\text{Cl} + \text{HCl} \rightarrow \text{ClH} + \text{Cl}$.

As previously noted by Broida, Tamir, and Persky,¹⁹ the O(³P) + HBr LEPS surface predicts substantial promotion of reactivity by HBr rotation. Although not investigated by Luntz and Andresen,⁷² we have found that the O(³P) + HR surface predicts a contrasting very dramatic decline in reactivity with rotation of the HR pseudodiatom. A very similar situation for two LEPS surfaces proposed²⁰ for the O(³P) + HCl system has recently been analyzed by Loesch.⁷⁵ His reduced dimensional analysis ("rotating sliding mass model"⁷⁶) of the surfaces illuminates the contrasting angular dependences of the entrance channel regions: it is clear that the rotational energy dependence of the reaction cross section is linked to similar factors to those controlling the product rotational energy distribution. When analyzed in the

(75) Loesch, H. *Chem. Phys.* **1987**, *112*, 85.

(76) Loesch, H. *Chem. Phys.* **1986**, *104*, 213.

rotating sliding mass formalism, the $O(^3P) + HBr$ and $O(^3P) + HR$ surfaces exhibit clearly the same qualitative differences identified by Loesch in the two $O(^3P) + HCl$ LEPS surfaces. We have performed further QCT calculations on the $O(^3P) + HBr$ and $O(^3P) + HR$ surfaces in which we have examined the correlation between reagent and product rotational energy distributions, but we do not present details of these studies in the present paper since we have not obtained equivalent experimental $O(^3P) + HBr$ data for comparison and the treatment of $O(^3P)$ is, in any case, physically unrealistic.

The preceding discussion offers a consistent explanation of the dynamics controlling H atom transfer reactions involving $O(^3P)$. Clearly, there is considerable scope for a more exact theoretical treatment of $O(^3P)$ hydrogen atom abstraction reactions. There is currently no substantiating evidence for the assumption of a direct collinear abstraction mechanism. It has been pointed out^{77,78} that there are qualitative similarities between the distributions obtained for the $O(^3P) + HBr$ reaction and certain reactions of $O(^1D)$, which almost certainly proceed by formation of an extremely short lived insertion intermediate. Holmlid and Elofson⁷⁹ have also suggested that the product energy partitioning can be reproduced by a statistical model with suitable constraints. Their calculations for $O(^3P) + HBr$ show good qualitative agreement with the experimental rotational distributions. However, we do not favor interpreting the $O(^3P) + HBr$ reaction as proceeding by a transient insertion mechanism. The extreme vibrational population inversion seems to be more consistent with a corner-cutting mechanism involving the direct abstraction of a light atom than a transient insertion intermediate. The calculation of accurate ab initio surfaces would facilitate the identification of the authentic mechanism of reaction. Further sophistications required in a more complete theoretical description include the rigorous treatment

of multisurface electronically nonadiabatic effects and the assessment of the importance of quantum mechanical tunneling.

Conclusion

The $O(^3P) + HBr \rightarrow OH(X^2\Pi) + Br$ reaction system has been investigated. The highly inverted vibrational and rotational distributions observed experimentally can be well-understood in terms of a direct abstraction mechanism for a heavy + light-heavy reaction dominated by kinematic constraints. QCT calculations on the $O(^3P) + HBr$ LEPS surface derived by Broida, Tamir, and Persky¹⁹ are capable of good qualitative, and in some respects quantitative, reproduction of the experimentally measured OH product state populations. The substantial rotational excitation of the OH product is dramatically different from the extremely cold rotational distributions observed in all previous H atom abstraction reactions by $O(^3P)$ with larger organic molecules (no rotational distributions have previously been measured for small inorganic molecules). The distinct dynamical behavior of the $O(^3P) + HBr$ and $O(^3P) + HR$ reactions can be rationalized in terms of different angular dependences of the model potential surfaces.

Acknowledgment. We are grateful to R. A. Copeland, J. B. Jeffries, and D. R. Crosley, and separately to J. R. Wiesenfeld and M. Troler, for providing OH transition probabilities in advance of publication. We thank M. D. Pattengill (University of Kentucky) and R. L. Jaffe (NASA Ames Research Center) for making available the computer code necessary for trajectory calculations and for useful discussions on its operation. Calculations were performed at the San Diego Supercomputer Center, using computer time granted via the U.S. National Science Foundation. K.G.McK. appreciates the award of a U.K. SERC Postdoctoral Research Fellowship. This work was supported by the U.S. National Science Foundation under Grant NSF CHE 87-05131.

Registry No. O, 17778-80-2; HBr, 10035-10-6; NO₂, 10102-44-0.

(77) Sloan, J. J. *J. Phys. Chem.* **1988**, *92*, 18.

(78) Kuntz, P. J.; Niefer, B. I.; Sloan, J. J. *J. Chem. Phys.* **1988**, *88*, 3629.

(79) See discussion of L. Holmlid and P. A. Elofson following ref 18.

Dynamics of Intramolecular Vibrational Energy Redistribution in Deuteriated Anthracenes: Rotational Band Contour Analysis and Time-Resolved Measurements

Lawrence W. Peng, Brian W. Keelan,[†] David H. Semmes, and Ahmed H. Zewail*[‡]

Arthur Amos Noyes Laboratory of Chemical Physics,[§] California Institute of Technology, Pasadena, California 91125 (Received: February 29, 1988)

The nature of intramolecular vibrational energy redistribution (IVR) in jet-cooled anthracene-9-*d*₁ and anthracene-*d*₁₀ has been investigated in both the frequency and time domains. Comparison with anthracene-*h*₁₀ is made, with particular emphasis on the role of vibrational density of states and molecular symmetry. The general regions of IVR (nonexistent, restrictive, and dissipative) have been identified, as in anthracene-*h*₁₀, in all molecules studied.

I. Introduction

In a recent series of papers published from this laboratory,^{1,2} the dynamics of intramolecular vibrational energy redistribution (IVR) was investigated in jet-cooled anthracene-*h*₁₀ and *trans*-stilbene. This was accomplished by spectrally and temporally resolving the fluorescence as a function of excess vibrational energy. From the spectral² data for anthracene-*h*₁₀, it was possible to assign the vibrational symmetries (*a*_g or *b*_{1g}) of levels below 1100 cm⁻¹ and other higher energy levels. In addition, the dis-

tinctiveness of the P-(Q)-R structure of the contours served as a basis for evaluating the spectral purity of levels, i.e., whether a level had major contributions from one (spectrally pure) or more than one (spectrally impure) vibronic state. The temporal data¹ revealed the dynamic nature of the redistribution as a function of excess energy. Single-exponential, quantum beats, and biexponential fluorescence decays have been measured for both anthracene-*h*₁₀ and *trans*-stilbene. The relationship of the decays to the nature of dynamic IVR (nonexistent to restrictive to dis-

[‡] John Simon Guggenheim Foundation Fellow.

[†] Present address: Eastman Kodak Research Laboratories, Rochester, NY 14650.

[§] Contribution no. 7743.

(1) (a) Felker, P. M.; Zewail, A. H. *J. Chem. Phys.* **1985**, *82*, 2961; (b) *Ibid.* 2975; (c) *Ibid.* 2994; (d) *Ibid.* 3003.

(2) Keelan, B. W.; Zewail, A. H. *J. Chem. Phys.* **1985**, *82*, 3011; *J. Phys. Chem.* **1985**, *89*, 4939.